How representative is a time series derived from a firn core? A study at a low-accumulation site on the Antarctic plateau

Lars Karlöf,[1,2] Dale P. Winebrenner,[3] and Donald B. Percival[3]

Received 5 May 2006; accepted 14 June 2006; published 13 October 2006.

[1] The acquisition and interpretation of increasingly high-resolution climate data from polar ice and firn cores motivates the question: What is the finest depth or timescale on which measurements on cores arrayed over a given area correlate? We analyze dated depth series of electrical and oxygen isotope measurements from a spatial array of firn cores with 3.5–7 km spacing in Dronning Maud Land, Antarctica, each with a temporal span of approximately 200 years. We use wavelet analysis to decompose the series into components associated with changes of averages on different scales, and thus deduce which scales are dominated by environmental noise, and which may contain a common signal. We find that common signals in electrical records have timescales of approximately 1–3 years. We identify only one electrical signal which rises significantly above the background in our 200-year records, evidently corresponding to the Tambora eruption. Several smaller signals correlate in a few of pairs of cores, one of which may correspond to a known volcanic event, but the others appear to be spurious. We present a simulation-based method for testing the significance of apparent electrical signal correlations, and highlight the importance of accurate relative dating between cores. In the case of oxygen-isotope records, we find, surprisingly, no significant correlation on any scale in the records, for any of the pairs of cores. There is, however, a weak trend toward positive correlation at longer timescales (up to 16 years). Statistical theory for the relevant confidence intervals and the observed statistics of the records permit estimation of the length of a data series necessary to reliably detect a hypothetical correlation equal to that observed. For the highest correlation observed on 16-year scales, core records of about 380 years (approximately 30 m at the Dronning Maud Land site) would be necessary to establish significance.

Citation: Karlöf, L., D. P. Winebrenner, and D. B. Percival (2006), How representative is a time series derived from a firn core? A study at a low-accumulation site on the Antarctic plateau, *J. Geophys. Res.*, *111*, F04001, doi:10.1029/2006JF000552.

1. Introduction

[2] Ice cores are believed to be one of the best noninstrumental climate archives available. The aim of analyzing an ice or firn core is usually to acquire precise data on climate, representative of some known area, with the highest possible temporal resolution. Ice cores record global and regional climate signals on millennial, centennial and, in some cases, decadal timescales [*EPICA Community Members*, 2004; *Petit et al.*, 1999; *Legrand and Mayewski*, 1997; *Mayewski et al.*, 1994; *Taylor et al.*, 1993; *Alley et al.*, 1993]. Technology now permits analysis of many ice and firn cores with much finer resolution in depth, and thus with annual and subannual resolution in time. However, short, transient signals may record very local variations in precipitation, wind-redistribution or other processes, which can obscure information about rapid climate variations. The questions thus arise: For cores arrayed over a given area, what is the finest temporal scale on which data, and thus climate inferences, correlate (i.e., how 'representative' is one core of another)? How does the degree of representation depend on the depth to which cores extend? Also, what can we infer from observations on a core array about the depositional or environmental differences between core sites that limit correlation? Addressing these questions can contribute to the analysis of many cores collected during traverse programs such as the International Trans-Antarctic Scientific Expedition (ITASE) [*Mayewski*, 2003] or European Project for Ice Coring in Antarctica (EPICA) [*Winther et al.*, 2002], which are designed to yield information on spatial variability in climate over short timescales.

[3] In this paper, we investigate the correlation between several time series obtained from EPICA firn cores (Figure 1) at five locations separated by distances between 3.5 and 7 km, on the polar plateau in Dronning Maud Land, East Antarctica [*Karlöf et al.*, 2005]. In particular, we examine

[1] Norwegian Polar Institute, Polar Environmental Centre, Tromsø, Norway.
[2] Now at Research and Development, Swix Sport AS, Lillehammer, Norway.
[3] Applied Physics Laboratory, University of Washington, Seattle, Washington, USA.

0148-0227/06/2006JF000552

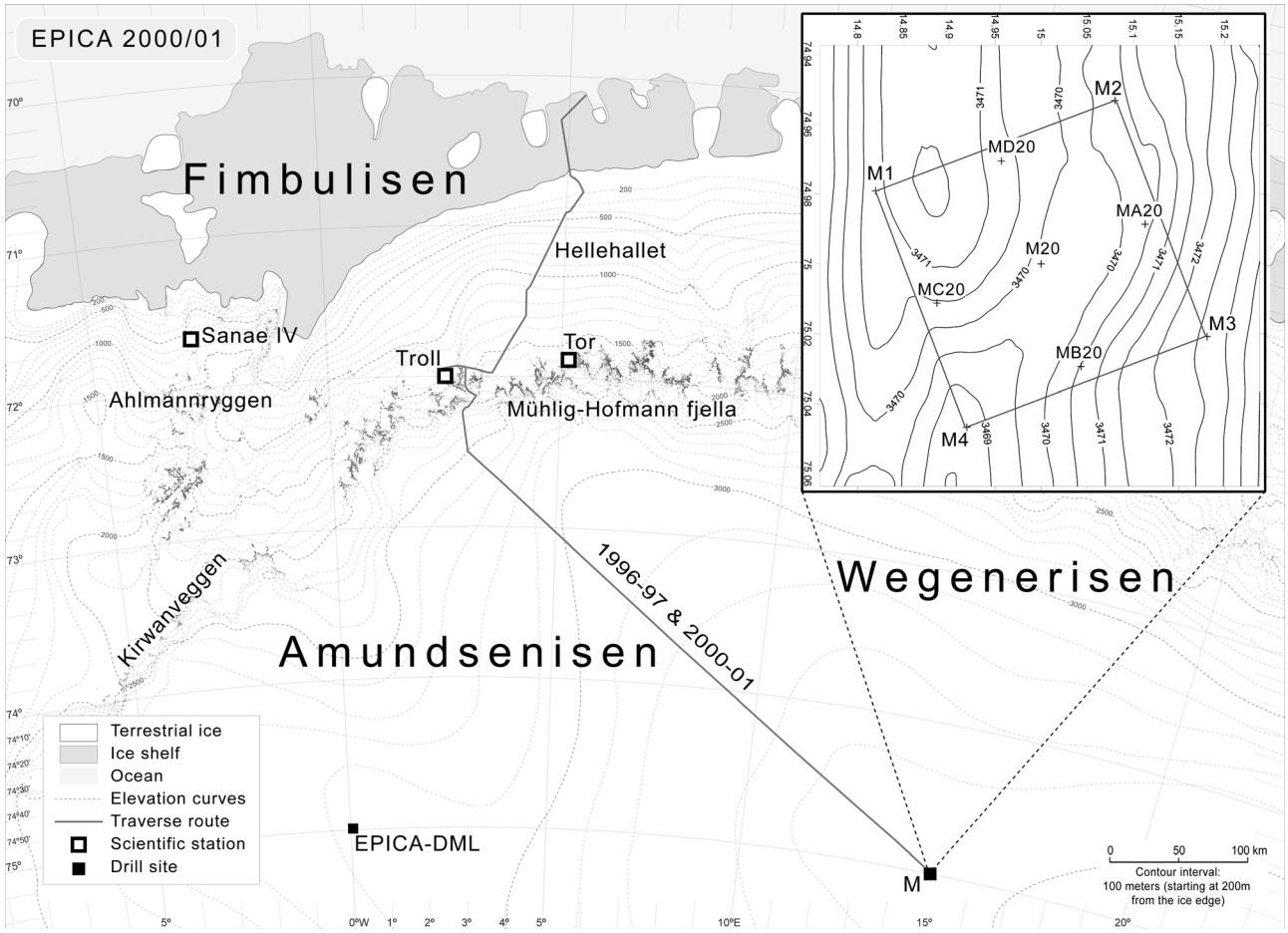

Figure 1. Study area in Amundsenisen, Dronning Maud Land, with detailed overview of the study area and local topography (inset). Drill sites are marked with a plus sign.

depth-series of Electrical Conductivity Measurement (ECM), Dielectric Profiling (DEP), and oxygen isotopes. On the Antarctic plateau, we consider the small spatial scale of this core array to be sufficient to exclude differences in records caused by different source area or large-scale precipitation patterns, different distances to the coast, or different temperatures caused by different elevations. Wind-driven redistribution of snow, however, is a potential cause of accumulation variability on these scales, and thus could cause variability in those firn core signals that are affected by accumulation.

[4] We address the question of degree of representation by using wavelet methods to analyze the core records. Wavelet methods have been applied to a wide variety of geophysical data series [e.g., *Percival and Mofjeld*, 1997; *Kumar and Foufoula-Georgiou*, 1997], including ones arising in glaciology [*Winebrenner et al.*, 2001]. The key idea is that depositional or postdepositional variability (i.e., 'environmental noise') acts differently at different scales in space and time, and thus will have scale-dependent influences on any signal that arises from the underlying (e.g., climate) dynamical process of interest. We use wavelet analysis to decompose the data series into components that are associated with changes of averages on different scales [*Percival and Walden*, 2000]. By comparing the wavelet decomposition of neighboring cores, we can deduce which scales are dominated by environmental noise and which scales may contain a common signal. In addition, wavelet analysis offers a scale- and time-based decomposition of the sample variance that allows us to identify time locations in the original series at which important changes occur. Finally, based on the large-sample statistical properties of wavelet coefficients, we can estimate to what depth a core must extend in order to have a reasonable chance of detecting (statistically) the presence of a common signal at a particular scale.

2. Data and Methods

2.1. Data

[5] In this study we have used electrical conductivity measurements (ECM), dielectrical profiling (DEP) and oxygen isotopes. After the records are dated and a time series is constructed, each record is trimmed to cover the same time period (183 years). Prior to the analysis the data is resampled to a constant sampling interval δ. The ECM record is block-averaged to the same sampling frequency as for the DEP in order to compare the electrical records on similar scales. This procedure can be regarded as low-pass filtering. For a full description of the data and area description we refer the reader to *Karlöf* [2004] and *Karlöf et al.* [2005].

[6] Conceptually the overall variance of a firn and ice core time series can be divided in two components, one attributable to a 'signal' (variations in the series that are in common with co-located core series) and the other, to 'noise' or local effects [*Fisher et al.*, 1985]. The noise could in principle be further divided into depositional and postdepositional components, but how exactly to quantify this decomposition is open to question. Fortunately this additional decomposition of the noise is of limited interest in this study since we are primarily interested in determining the scales at which the signal is dominant.

2.2. Wavelet Methods

[7] Changes in accumulation will likely result in firn core time series whose underlying mean and variance are changing with time, which means such series cannot be modeled globally as realizations of a stationary process. In recent years wavelet methods have emerged as useful alternatives to Fourier-based methods for analyzing time series with time-varying characteristics. Both methods proceed by transforming the time series under study into a collection of new values known as coefficients. The key reason that wavelet analysis is more useful than Fourier analysis for series with time-varying characteristics is that wavelet coefficients are influenced by local events in a series, whereas Fourier coefficients depend upon the entire series [*Kumar and Foufoula-Georgiou*, 1997]. In this study we have used a version of the discrete wavelet transform (DWT) known as the maximal overlap DWT (MODWT). The MODWT is a decomposition of a time series on a scale-by-scale basis, yielding localized coefficients that can then be compared with those of other time series to ascertain the correlation structure on a scale-by-scale basis. Unlike the usual orthogonal DWT, which is naturally defined only for series whose sample sizes are a multiple of a power of 2, the MODWT is well defined for all sample sizes, which is convenient here because our sample sizes typically do not satisfy the required constraint (one way of using the orthogonal DWT would be to truncate our series down to an acceptable sample size, but this is unappealing because our series are already short as is). The MODWT is not an orthogonal transform, but, as we note below, it can be used to construct a multiresolution analysis and an analysis of variance that parallel those given by the orthogonal DWT. In what follows, we give a brief description of the MODWT. We refer the reader to chapters 5 and 8 of *Percival and Walden* [2000] and references therein for more details.

[8] Consider a time series of regularly spaced data that we express as a vector $\mathbf{X}$ of length N with elements $X_0, X_1, \ldots, X_{N-1}$. The MODWT wavelet coefficients for a particular scale (indexed by a positive integer j) are obtained by circularly filtering $\mathbf{X}$ with a wavelet filter $\{\tilde{h}_{j,l}\}$ of width L_j:

$$\widetilde{W}_{j,t} = \sum_{l=0}^{L_j-1} \tilde{h}_{j,l} X_{t-l \bmod N}, \ t = 0, 1, \ldots, N-1. \tag{1}$$

The physical scale for these coefficients is given by $\lambda_j = 2^{j-1}\,\delta$, where δ is the sampling interval between observations (for example, $\delta = 0.05$ years for the time series shown in Figure 2). The MODWT wavelet coefficients can be interpreted as being proportional to changes between two adjacently located and possibly weighted averages of the time series, with the effective width of both averages being λ_j. If we place the MODWT coefficients in a vector $\widetilde{\mathbf{W}}_j$, we can express the above in matrix notation as

$$\widetilde{\mathbf{W}}_j = \mathcal{W}_j \mathbf{X}, \tag{2}$$

where $\mathcal{W}_j$ is the $N \times N$ transformation matrix for scale λ_j (its elements are dictated entirely by $\{\tilde{h}_{j,l}\}$).

[9] Let us now consider the wavelet coefficients $\widetilde{\mathbf{W}}_j$ indexed by $j = 1, 2, \ldots, J_0$, where J_0 is a positive integer whose choice is application dependent. We can use these coefficients to form a decomposition of the 'energy' $\|\mathbf{X}\|^2 \equiv \sum_{t=0}^{N-1} X_t^2$ in our time series if we make use of one additional vector $\widetilde{\mathbf{V}}_{J_0}$, the so-called scaling coefficients for scale $2\lambda_{J_0}$. The elements of this vector are formed by circularly filtering $\mathbf{X}$ with a scaling filter $\{\tilde{g}_{J_0,l}\}$ of width L_{J_0}:

$$\widetilde{V}_{J_0,t} = \sum_{l=0}^{L_{J_0}-1} \tilde{g}_{J_0,l} X_{t-l \bmod N}, \ t = 0, 1, \ldots, N-1. \tag{3}$$

Placing these coefficients into the vector $\widetilde{\mathbf{V}}_{J_0}$, we can reexpress the above as

$$\widetilde{\mathbf{V}}_{J_0} = \mathcal{V}_{J_0} \mathbf{X}, \tag{4}$$

where $\mathcal{V}_{J_0}$ is a suitably defined $N \times N$ transformation matrix. These scaling coefficients can be interpreted as being proportional to localized and possibly weighted averages of the time series, with the effective width of the average being $2\lambda_{J_0}$. The desired energy decomposition takes the form

$$\| \mathbf{X} \|^2 = \sum_{j=1}^{J_0} \| \widetilde{\mathbf{W}}_j \|^2 + \| \widetilde{\mathbf{V}}_{J_0} \|^2 . \tag{5}$$

In words, $\|\widetilde{\mathbf{W}}_j\|^2$ is the contribution to the energy in the time series that is attributable to changes in averages over the physical scale λ_j, while $\|\widetilde{\mathbf{V}}_{J_0}\|^2$ is the contribution due to averages over scale $2\lambda_{J_0}$.

[10] Since the sample variance for $\mathbf{X}$ is given by

$$\hat{\sigma}_X^2 = \frac{1}{N} \| \mathbf{X} \|^2 - \overline{X}^2, \text{ where } \overline{X} = \frac{1}{N} \sum_{t=0}^{N-1} X_t, \tag{6}$$

we can form a scale-by-scale decomposition of the sample variance via

$$\hat{\sigma}_X^2 = \frac{1}{N} \sum_{j=1}^{J_0} \| \widetilde{\mathbf{W}}_j \|^2 + \frac{1}{N} \| \widetilde{\mathbf{V}}_{J_0} \|^2 - \overline{X}^2. \tag{7}$$

The terms $\frac{1}{N}\|\widetilde{\mathbf{W}}_j\|^2$ and $\frac{1}{N}\|\widetilde{\mathbf{V}}_{J_0}\|^2 - \overline{X}^2$ can be regarded as the components of a wavelet power spectrum, which decomposes the variance of $\mathbf{X}$ into variations on distinct scales. In particular, the last of these terms is just the sample variance of the scaling coefficients (the term $\frac{1}{N}\|\widetilde{\mathbf{W}}_j\|^2$ can

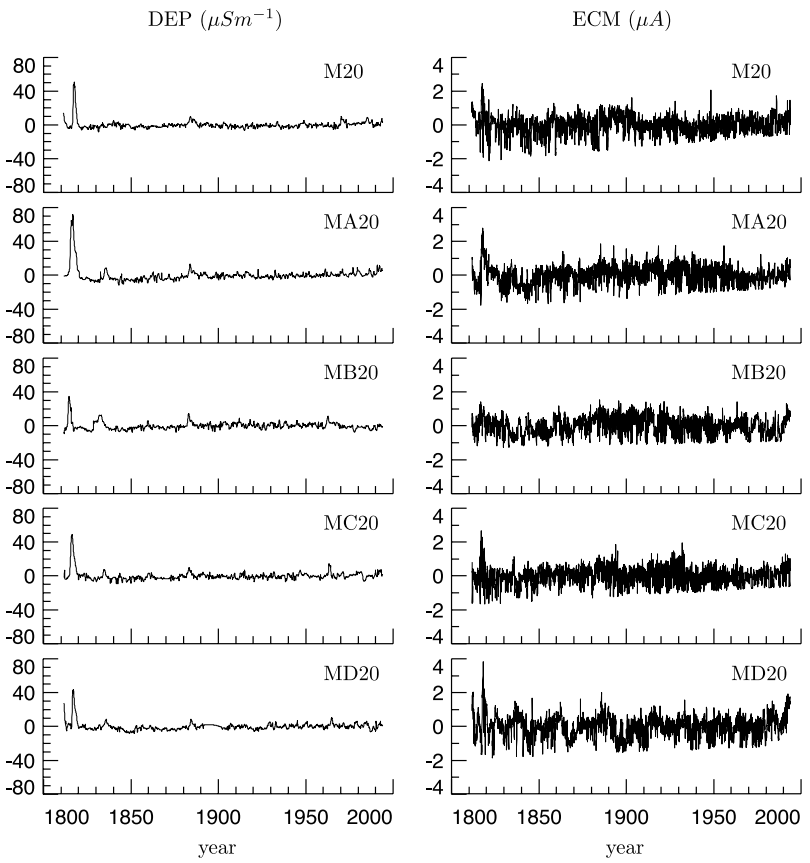

Figure 2. DEP and ECM records (left- and right-hand columns, respectively) from the five cores. The sampling interval δ is 0.05 years for both records. The different amplitudes and shapes of the peaks are an effect of snow depositional processes at the drill site. The DEP data were sampled every 5 mm with a 10-mm electrode, which effectively acts as a low-pass filter, resulting in a higher signal-to-noise ratio.

also be regarded as a sample variance because there are theoretical reasons for assuming that the population mean of $\widetilde{\mathbf{W}}_j$ is zero).

[11] In addition to forming a wavelet power spectrum, we can use the MODWT coefficients to create an additive decomposition of $\mathbf{X}$ that is known as a multiresolution analysis (MRA). The components of an MRA are J_0 'detail' time series for scales λ_j, $j = 1, 2, \ldots, J_0$, defined as

$$\widetilde{\mathcal{D}}_j \equiv \mathcal{V}_j^T \widetilde{\mathbf{W}}_j, \tag{8}$$

along with a 'smooth' series for scale $2\lambda_{J_0}$, defined as

$$\mathcal{S}_{J_0} \equiv \mathcal{V}_{J_0}^T \widetilde{\mathbf{V}}_{J_0}. \tag{9}$$

The desired additive decomposition of $\mathbf{X}$ is

$$\mathbf{X} = \sum_{j=1}^{J_0} \widetilde{\mathcal{D}}_j + \widetilde{\mathcal{S}}_{J_0}. \tag{10}$$

In words, an MRA reexpresses $\mathbf{X}$ as the sum of $J_0 + 1$ new time series, the first J_0 of which (the details) are associated with changes on scales λ_1 up to λ_{J_0}, while the last one (the smooth) is associated with averages over the scale $2\lambda_{J_0}$. The details $\widetilde{\mathcal{D}}_j$ and smooth $\widetilde{\mathcal{S}}_{J_0}$ are both associated with zero phase filters, which ensures that features in an MRA are aligned properly with the corresponding time series. (It should be noted that the wavelet and scaling coefficients themselves are not outputs from zero phase filters, but can be regarded approximately as such for certain wavelet filters if the coefficient vectors $\widetilde{\mathbf{W}}_j$ and $\widetilde{\mathbf{V}}_{J_0}$ are circularly shifted appropriate amounts. Without these shifts, features in the coefficients will not line up properly with features in the time series.)

[12] Because we are interested in the correlation between two different firn cores on a scale-by-scale basis, we also consider a sample wavelet cross correlation as a standardized covariance between wavelet coefficients for two time series $\mathbf{X}$ and $\mathbf{Y}$ at a given scale:

$$\hat{\rho}_{XY,j} \equiv \frac{\sum_{t=0}^{N-1} \widetilde{W}_{X,j,t} \widetilde{W}_{Y,j,t}}{\| \widetilde{\mathbf{W}}_{X,j} \| \cdot \| \widetilde{\mathbf{W}}_{Y,j} \|}, \tag{11}$$

where $\widetilde{\mathbf{W}}_{X,j}$ and $\widetilde{\mathbf{W}}_{Y,j}$ contain the MODWT wavelet coefficients for scale λ_j for, respectively, $\mathbf{X}$ and $\mathbf{Y}$, and the elements of these two vectors are denoted by, respectively, $\widetilde{W}_{X,j,t}$ and $\widetilde{W}_{Y,j,t}$. In words, $\hat{\rho}_{XY,j}$ tells us how correlated the series $\mathbf{X}$ and $\mathbf{Y}$ are at scale λ_j and allows us to study the relationship between the two series on a scale-by-scale

basis. This statistic is roughly analogous to the sample magnitude-squared coherence from Fourier analysis.

[13] The wavelet power spectrum, the MRA and the sample wavelet cross-correlation are the wavelet-based decompositions and sample statistics that we use in this paper. How exactly we use them involves some adaptation of the material discussed above. First, note that equations (7) and (11) use all available MODWT wavelet coefficients (we will ignore the portion of the wavelet power spectrum due to the scaling coefficients because it is not of direct interest). Some of these coefficients, the so-called boundary coefficients, can be adversely affected by the circular filtering operation that is inherent in the MODWT (see *Percival and Walden* [2000] for details). By definition the boundary coefficients are those whose values would in general change if we were to eliminate the modulo operation in equations (1) and (3). Including these nonboundary coefficients can lead to unacceptable biases, but this defect can be mitigated if we use reflection boundary conditions instead. This involves taking the original series of length N and concatenating it with a reversed version of the series to form an extended series of length $2N$, namely, $X_0, X_1, \ldots, X_{N-2}, X_{N-1}, X_{N-1}, X_{N-2}, \ldots, X_1, X_0$. This series necessarily has the same sample mean and variance as the original series $\mathbf{X}$; however, by construction, the beginning and end of the extended series match up well, whereas this need not be the case for the original series, which can lead to large biases in the boundary coefficients. The extended series is then analyzed in place of the original series in the manner described above. Biases due to the circularity assumption are largely mitigated, and computer experiments indicate that the resulting estimators $\frac{1}{N}\|\widetilde{\mathbf{W}}_j\|^2$ and $\hat{\rho}_{XY,j}$ have smaller mean squared errors than ones using just the non-boundary wavelet coefficients. Under certain assumptions, both estimators have an associated population value, and confidence intervals for the unknown population value can be computed based upon these estimators. We make use of these confidence intervals in Figures 6 and 7 in section 3.2. Computation of these intervals is discussed in detail by *Percival and Walden* [2000] and *Whitcher et al.* [2000] for estimators that make use of just the nonboundary coefficients, but asymptotically these estimators have the same large sample properties as ones formed using all the coefficients and reflection boundary conditions.

[14] The results of a wavelet analysis will depend (to some degree at least) on the particular set of wavelet filters used. The wavelet and scaling filters $\{\tilde{h}_{j,l}\}$ and $\{\tilde{g}_{J_0,l}\}$ for $j \geq 2$ and any J_0 depend just on the choice of the wavelet filter $\{\tilde{h}_{1,l}\}$ for scale λ_1. We considered three different wavelets $\{\tilde{h}_{1,l}\}$, the Haar wavelet, the Daubechies extremal phase wavelet of width $L_1 = 4$ (D(4)) and the Daubechies least asymmetric wavelet of width $L_1 = 8$ (LA(8)). When choosing an appropriate wavelet, we considered the introduction of undesired artifacts (more artifacts with shorter wavelets), the number of coefficients influenced by boundary conditions (more with longer wavelets) and the localization in time (less with longer wavelets). We choose to use the D(4) wavelet as a compromise between the extremes offered by the Haar and LA(8) wavelets, but the results of our analysis are virtually the same using the other two wavelets. The maximum level out to which we computed the MODWT was $J_0 = 9$ for the electrical data and $J_0 = 6$ for the ^{18}O data.

3. Results

3.1. Records of Electrical Conductivity Measurements and Dielectrical Profiling

[15] Firn and ice core ECM and DEP records display narrow excursions, i.e., spikes, above a background. These spikes are typically associated with historical depositions on the ice sheet surface of volcanic acid and, in the case of DEP, other ions [*Moore et al.*, 1992; *Wolff et al.*, 1995]. Between spikes, the records are typically relatively quiescent; i.e., the sample means and variances change only slowly with depth, and correlations between samples decay rapidly with increasing lag (although records with subannual temporal resolution can be used to identify annual layering [*Taylor et al.*, 2004]). The depths of spikes in a firn and ice core, together with dating of volcanic inputs, enable the derivation of climate information such as accumulation rate histories.

[16] Figure 2 shows the DEP and ECM records for the five EPICA cores used in this study, after removal of variations in both records on the scale of the record length that are unrelated to volcanic inputs. We have first corrected the DEP data for a known variation with firn density, following the standard procedure described by *Hofstede et al.* [2004], and further removed a linear trend with depth. Second, we have removed a linear trend with depth in the ECM records, which is thought to result from decreasing contact resistance at the ECM electrodes as a function of firn density (although the physics underlying this effect remain poorly understood [*Karlöf et al.*, 2000]). This preprocessing of DEP and ECM records helps to eliminate artifacts in the MRAs due to the circularity assumption used in forming the MODWT coefficients (equations (1) and (3)).

[17] All the records in Figure 2 show their largest event at approximately the year 1815, which was the year of the volcanic eruption of Tambora. The duration of this event in each record is a few years. All of the DEP records also show a smaller candidate event of a few years in duration, around 1883, which was the year of the Krakatoa eruption. (For brevity, we will henceforth refer to the ca. 1815 and 1883 events as the Tambora and Krakatoa events, respectively, while noting that conclusive identification of events with eruptions can only result from detailed analysis that lies beyond the scope of this paper.) The high noise levels in the ECM records make visual identification of the Krakatoa event problematic. The apparent commonality of event durations in the records, however, suggests analysis of signal characteristics in terms of temporal scale.

[18] Figure 3 shows wavelet power spectra for the DEP and ECM records. Each of the DEP spectra shows a peak on a scale of either 1.6 or 3.2 years, corresponding to the approximate durations of the Tambora and Krakatoa events in the records. The high levels of small-scale noise in ECM records could be obscuring peaks at these scales in 3 of the 5 ECM spectra, but data from cores MA20 and MD20 do show either a local or global peak at 3.2 years. We interpret this as confirmation that the predominant scales for signals in electrical records occur at 1.6 to 3.2 years. We are thus motivated to construct a partial multiresolution analysis

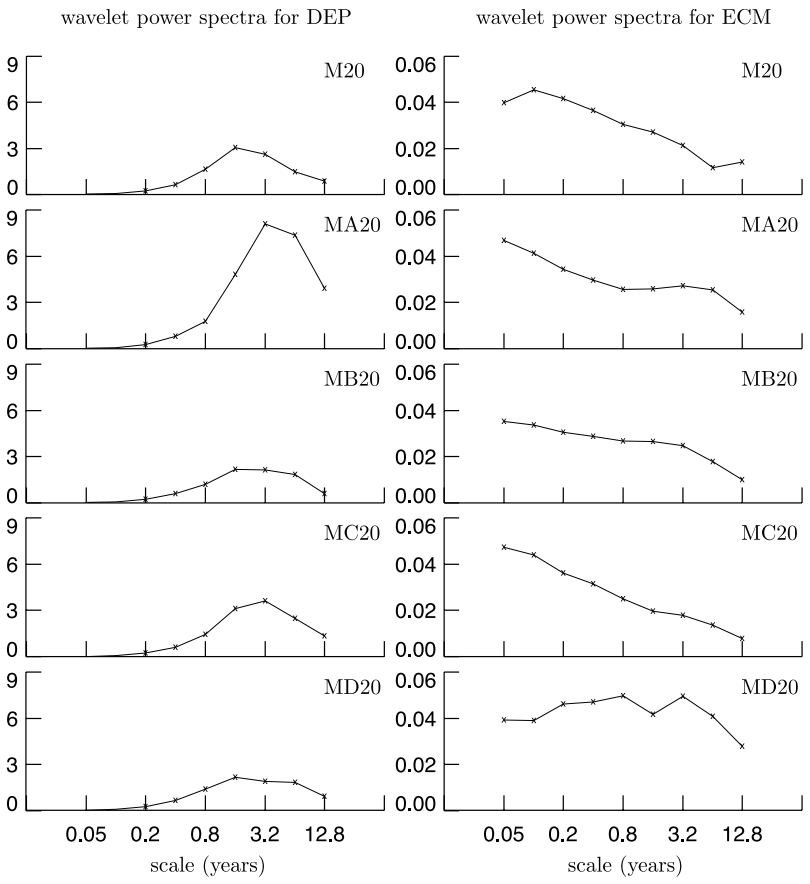

Figure 3. Wavelet power spectra for DEP and ECM records (left- and right-hand columns, respectively) from the five cores. These plots depict the decomposition of the sample variance for each record across the scales $\lambda_j\delta = 0.05 \times 2^{j-1}$ years, where $j = 1, \ldots, 9$. The spectra are based upon the Daubechies $D(4)$ wavelet and a MODWT using reflection boundary conditions as applied to the residuals from a linear least squares fit to a given record. Note that small-scale noise is the dominant contributor to the sample variance for the ECM records, whereas dominant scales for the DEP records are 1.6 and 3.2 years.

consisting of the sum of the details $\widetilde{\mathcal{D}}_6$ and $\widetilde{\mathcal{D}}_7$, corresponding to 1.6 and 3.2 years, respectively. This sum of details constitutes one way to 'denoise' the individual records, and serves also as a basis for a scale-dependent correlation analysis. Figure 4 shows $\widetilde{\mathcal{D}}_6 + \widetilde{\mathcal{D}}_7$ for DEP and ECM records. The Tambora event dominates each record in these figures as well, but lower noise levels here show additional candidate events more clearly. Slight uncertainties in core dating may also be apparent in, for example, the slightly later occurrence of the Tambora event in the record from core M20, compared to the other DEP (though not ECM) core records.

[19] Consider first the results from DEP records (left-hand column of Figure 4). The solid vertical lines in each plot mark the years 1815, 1883 and 1965 (the dashed lines result from analysis of the ECM records, to be discussed momentarily). The relatively small Krakatoa event (1883) again appears in each record, somewhat more cleanly here than in the originals. A candidate event also occurs in all cores except MA20 around 1965, with greater clarity than in the original records, and with magnitude similar to the Krakatoa event. The occurrence in core M20 is at 1970, which is noticeably later than at the other cores recording this event. The Tambora event for core M20 also occurs slightly 'late.' The failure of the 1965–1970 event to appear in the record from MA20 suggests that events with magnitudes (relative to background) near those of the Krakatoa and 1965–1970 events may be near some limit, below which recording in the firn is unreliable within even a small area, i.e., below which a signal (or lack of signal) in a single ice core is not representative. If so, we would expect the relatively noisy ECM records to show less correlation than the corresponding DEP records.

[20] Correlations between ECM records are not obvious, however, even after wavelet denoising (right-hand column of Figure 4). To address this, we have estimated the statistical significance of correlations between variations on scales $j = 6$ and 7 in the various ECM records. Briefly, we used apparently quiescent periods in the ECM series to develop a model for eventless noise, and established limits that trap the entire scatterplot of two ECM records of $\widetilde{\mathcal{D}}_6 + \widetilde{\mathcal{D}}_7$ with probability 0.95 under the null hypothesis that the two records are uncorrelated. Excursions outside of these limits in the actual records identify localized events that are worthy of further study. (Full details are given in Appendix A.) Only four such events were identified by this procedure.

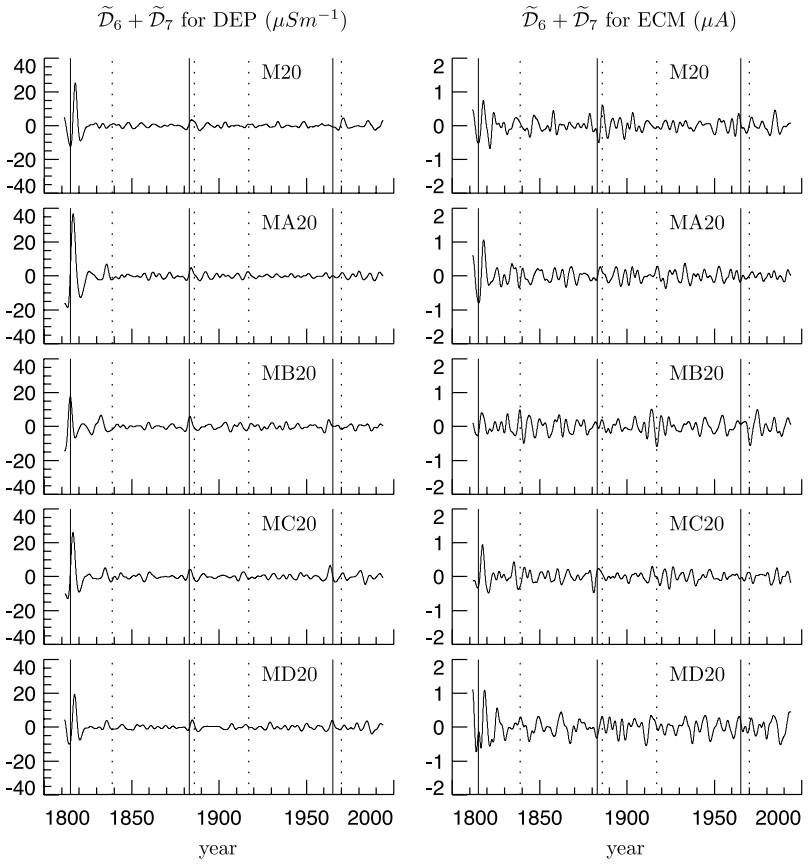

Figure 4. Sum of MODWT details $\widetilde{\mathcal{D}}_6$ and $\widetilde{\mathcal{D}}_7$ for DEP and ECM records (left- and right-hand columns, respectively) from the five cores, computed using the same setup for the MODWT as described for Figure 3. Collectively, these two details capture variations on scales of 1.6 and 3.2 years. The solid vertical lines on each plot mark the years 1815 (the Tambora event), 1883 (the Krakatoa event), and 1965; the dotted vertical lines mark 1839, 1886, 1917, and 1970.

Their times are indicated in all of the plots in Figure 4 by dashed vertical lines. The Krakatoa event appears as a statistically significant event in only 3 of the 10 possible pairings of ECM records, namely M20 vs. MA20, M20 vs. MB20, and M20 vs. MC20. What may be the 1965–1970 event, albeit shifted systematically in time, is significantly correlated in 3 parings (M20 vs. MB20, MA20 vs. MB20, and MB20 vs. MC20) as well. The possible time-shift of this event highlights the importance of core dating to our correlation analysis, as shown in Appendix A, oscillations in neighboring cores of similar wave-form but differing phases can easily fail to correlate.

[21] Given the noise characteristics and dating accuracies of ECM records in this study, we infer a single firn core is not representative of events of the strength of Krakatoa. We also find, however, apparently spurious correlations in 5 pairings. Three of these involve MB20 in the year 1917. Visual examination of the MB20 record shows that the spurious correlations are induced by a burst of noise in that record around 1917. The other two involve MB20 in 1839 and have a similar interpretation. Thus the dangers of interpreting small events in a single firn core include 'finding' events that would not be recorded elsewhere, as well as missing events that would appear in data from a more extensive array of cores.

3.2. Oxygen Isotopes

[22] Oxygen isotope records differ strongly from the electrical records in both character and detail. Figure 5 shows the oxygen isotope records for each of the 5 cores, together with the corresponding wavelet power spectra. Detailed descriptions of the data are given by *Karlöf* [2004] and *Karlöf et al.* [2005]. Three of the records show maximum variance at the 2-year timescale, and the other two, at 4 years (although one of these (MA20) has nearly identical variances at the 2- and 8-year timescales). The variances in the records are not, however, homogeneous over the lengths of the records. Figure 6 shows, for each core, the series of wavelet coefficients on scales indexed by $j = 1$ and 3 (0.5 and 2 years) over the length of the record, as well as wavelet power spectra computed separately for the first and second halves of the record (circles and crosses, respectively) with associated 95% confidence intervals. The apparent damping with increasing age of variance on scales of 0.5 to 2 years is consistent, at least qualitatively, with the diffusion of oxygen isotopes after deposition [*Johnsen et al.*, 2000; *Rempel et al.*, 2001; *Rempel and Wettlaufer*, 2003].

[23] The oxygen isotope records from separate cores do not, however, correlate on the timescales where most of the variance occurs. Rather, we observe a weak trend toward

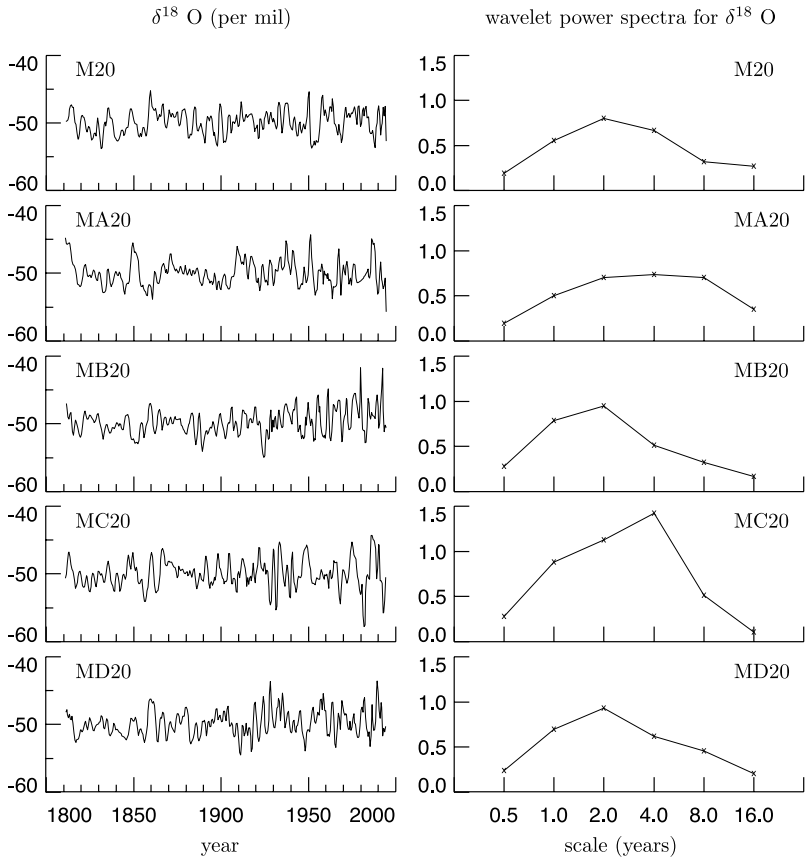

Figure 5. Oxygen isotope records and corresponding wavelet power spectra (left- and right-hand columns, respectively) from the five cores. The sampling interval δ is 0.52 years. The spectra are based upon the Daubechies $D(4)$ wavelet and a MODWT using reflection boundary conditions applied to each displayed record.

positive correlation increasing timescales, in just 3 of the 10 possible pairwise correlations (Figure 7). In no case do the observed correlations reach statistical significance. Thus, surprisingly, we find no strong evidence of correlation between any of these 5 closely spaced core records on any timescale up to and including the longest timescale in the records, 183 years. Because of the strong, well-established link between oxygen isotopes and temperature on longer timescales [*Petit et al.*, 1999], we are motivated to ask what the shortest timescale would be on which we could expect to test for statistically significant correlation, given the statistical properties exhibited by our 183 year records. We address this question in the following section.

4. Discussion and Concluding Remarks

[24] The data in section 3 show that the degree to which a signal in a given core occurs also in neighboring cores depends on the nature (e.g., electrical versus isotopic), scale and magnitude of that signal; that is, an answer the question 'How representative is an ice core?' requires that we specify carefully what representation we seek. The data presented here clarify the necessary specifications in the cases of electrical and oxygen-isotope data, but further work is required both for complete, quantitative specification at the EPICA site, and to understand the depositional, climatic and other factors that may affect specifications in other locations.

[25] In the case of electrical data, and especially ECM data, the size of an event is clearly a strong determinant of whether it is found in neighboring records as well. From the limited data presented here, it appears that the size threshold, above which an event is likely to correlate, is somewhat larger than that of the event (likely) owing to the eruption of Krakatoa. Examination of the events in Figure 4 shows, however, that event size is variable between cores. Thus further observations are needed to characterize such variability quantitatively. Such characterization could then be combined with the results in Appendix A to quantify the probability that events of given mean magnitude in separate core records would correlate significantly. A prerequisite, however, to any such work will be verification that the uncertainties in depth and depth-age scales for the ice cores involved are, or can be made, small in comparison to scales on which most of the signal energy occurs.

[26] Our ability to detect significant global correlations at a given scale between pairs of cores is necessarily limited by the length of the core. To explore the effect of core length, note that, in Figure 7, the largest observed wavelet cross-correlation $\hat{\rho}_{XY,j}$ occurs between the MA20 and MC20 ^{18}O series at a 16-year scale, for which $j = 6$. Since we are using the D(4) wavelet, an approximate 95% confidence

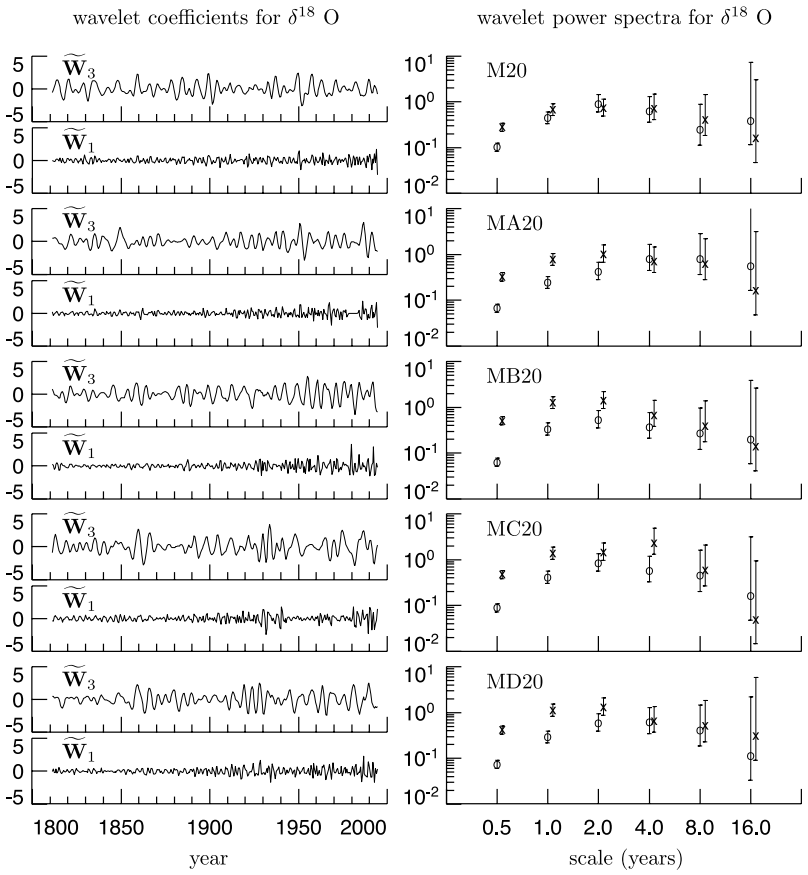

Figure 6. (left) Time-aligned wavelet coefficients at scales indexed by $j = 1$ and 3 for the oxygen isotope records from the five cores, along with (right) wavelet power spectra at all scales for the first and second half of each record (circles and crosses, respectively). The wavelet coefficients and spectra are based upon the Daubechies $D(4)$ wavelet and a MODWT using reflection boundary conditions. The spectra are plotted along with 95% confidence intervals. Note that the variability in $\widetilde{\mathbf{W}}_1$ increases with time for all five cores, which is confirmed by the fact that the 95% confidence intervals for the spectra for two halves do not overlap. The tendency for variability to increase with time dissipates as the scale increases.

interval based upon the estimate $\hat{\rho}_{XY,6} \doteq 0.65$ is given by [*Whitcher et al.*, 2000]

$$\left[\tanh\left\{\tanh^{-1}(0.65) - \frac{1.96}{\sqrt{(\frac{N}{64}-5)}}\right\} \quad \tanh\left\{\tanh^{-1}(0.65) + \frac{1.96}{\sqrt{(\frac{N}{64}-5)}}\right\}\right].$$

[27] The resulting interval $[-0.96, 1.0]$ is very wide and traps zero, so, at the 0.05 level of significance, we certainly cannot reject the null hypothesis that the corresponding population cross correlation $\rho_{XY,6}$ is zero. Suppose, however, that the population cross correlation $\rho_{XY,6}$ were actually equal to the observed cross correlation and that, if we had more data available to us, we would still get an estimate of $\hat{\rho}_{XY,6} \doteq 0.65$. Given this scenario, we can determine how large N must be so that the lower limit of the 95% confidence interval would result in our just being on the borderline of rejecting the null hypothesis; that is, we want to determine N such that the lower limit of the 95% confidence interval is zero. Setting the expression for this lower limit to zero and solving for N yields

$$N = 64\left(\frac{1.96}{\tanh^{-1}(0.65)}\right)^2 + 320 \doteq 729.$$

Since $\delta \doteq 0.52$ years for the ^{18}O series, we would need to have a series covering about 380 years to have enough statistical evidence to be able to (just barely) reject the null hypothesis of zero cross correlation. At this site this corresponds to a core that would be approximately 30 m deep.

[28] Finally, a general understanding of signal correlation will require understanding of the physical mechanisms, both depositional and post-depositional, that underlie signal variability. One site may be eroded in the beginning of a precipitation event, whereas another is eroded later. This may explain how localized events in time can be anti-correlated in the scale-by-scale correlation study. Moreover, the probability of eroding a 'significant' amount of snow related to a certain event is dependent on wind, temperature, initial snow density, thickness of snow layer and the time

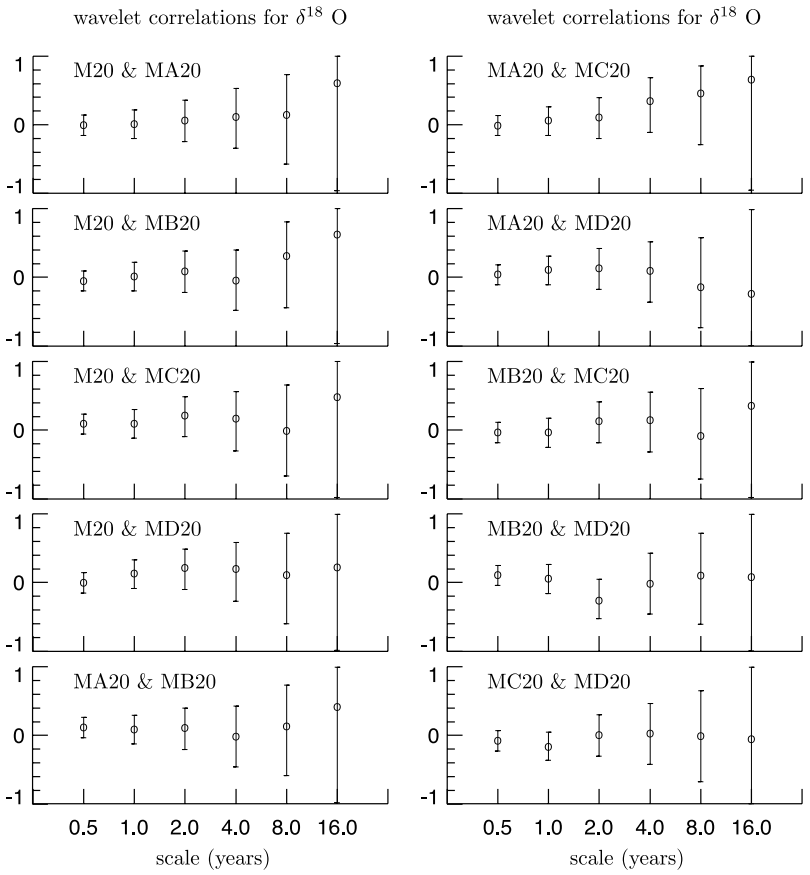

Figure 7. Wavelet cross correlations at lag $\tau = 0$ for the ten possible pairings of the five oxygen isotope records, along with 95% confidence intervals. These are based upon the Daubechies $D(4)$ wavelet and a MODWT using reflection boundary conditions.

elapsed between deposition and erosion. (The small spatial scale considered in this study suggests disregarding temperature and elapsed time as causes, leaving initial snow density and thickness of snow layer as the important factors in this study.) Study of these questions may require multiyear experiments with core arrays and detailed meteorological records to compare conditions of signal incorporation with the actual signals that remain in cores.

Appendix A

[29] Here we give details about how we ascertained the significance of localized correlations in $\widetilde{\mathcal{D}}_6 + \widetilde{\mathcal{D}}_7$ between pairs of ECM series, for example, M20 and MA20. For each core we subtracted off a line determined by linear least squares to obtain a set of residuals, say, $r_0, r_1, \ldots, r_{N-1}$, where here $N = 3666$. We fit a first-order autoregressive (AR) model to the middle half of these residuals, i.e., r_{916}, $r_{917}, \ldots, r_{2748}$, using Burg's algorithm [*Percival and Walden*, 1993]. Using just the middle half ensures that the fitted AR model is focused on the apparently quiescent portions of both series. We also considered higher-order AR models, but found a first-order model to adequately describe the correlation properties for all five cores. We then simulated a pair of Gaussian distributed series [*Kay*, 1981], one using the fitted model for M20, and the other, for MA20. While each series is autocorrelated, the two series were generated independently of each other, and hence any apparent localized correlations at any given scale between the simulated series are due to sampling variations, and not to an actual coupling between the two series. We then computed $\mathcal{U} \equiv \widetilde{\mathcal{D}}_6 + \widetilde{\mathcal{D}}_7$ for both simulated series. Let $\mathcal{U}_t^{(\mathrm{M20})}$ be the tth element of $\mathcal{U}$ for the series simulated using the AR model for M20, and let $\mathcal{U}_t^{(\mathrm{MA20})}$ be the corresponding quantity for MA20. We determined the ellipse such that all values of $\mathcal{U}_t^{(\mathrm{M20})}$ versus $\mathcal{U}_t^{(\mathrm{MA20})}$, $t = 0, \ldots, N-1$, were contained within or on the ellipse, with a least one point being on the ellipse. The ratio of the semimajor and minor axes of the ellipse was dictated by the ratio of the observed standard deviations of the M20 and MA20 series; this is quite close to unity, so the ellipse is close to being a circle. We repeated this procedure 10,000 times, which allows us to empirically determine how well we can expect $\mathcal{U}_t^{(\mathrm{M20})}$ to match up locally with $\mathcal{U}_t^{(\mathrm{MA20})}$ when in fact the M20 and MA20 series are uncorrelated.

[30] The dots in Figure A1 show the scatterplot of $\mathcal{U}_t^{(\mathrm{M20})}$ versus $\mathcal{U}_t^{(\mathrm{MA20})}$ for the actual data, along with two ellipses. The inner (outer) ellipse is the ellipse that trapped 95% (99%) of scatterplots for the 10,000 simulated pairs. There are five excursions in the actual data outside of the 99% ellipse, and these are labeled on the plot with the year of the point $(\mathcal{U}^{(\mathrm{MA20})}{}_t, \mathcal{U}_t^{(\mathrm{M20})})$ that lies furthest from the origin. Significant locally correlated events in the actual cores should tend to fall close to a 45° line through the origin of the plot. If the event is displaced in time in one of the cores due to uncertainty in matching depth with age, points

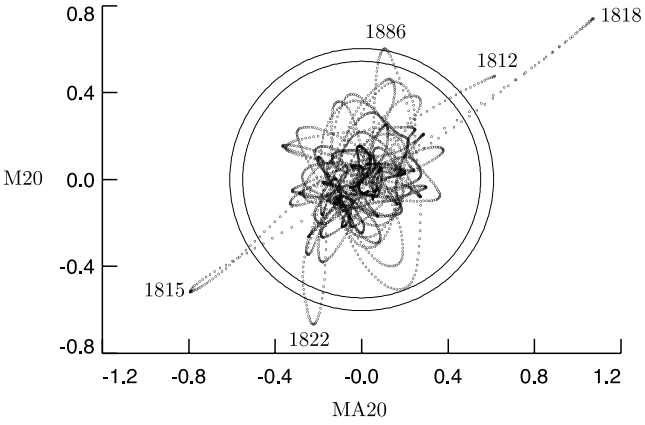

Figure A1. Scatterplot of $\widetilde{\mathcal{D}}_6 + \widetilde{\mathcal{D}}_7$ for the M20 ECM record versus the same sum of details for the MA20 record. The details are based upon the Daubechies $D(4)$ wavelet and MODWTs using reflection boundary conditions. The points in the scatterplot are formed by plotting the tth element of $\widetilde{\mathcal{D}}_6 + \widetilde{\mathcal{D}}_7$ for the M20 ECM record (top right-hand plot in Figure 4) versus the corresponding element for the MA20 ECM record (second plot in the right-hand column). The inner and outer rings depicts 95% and 99% confidence limits for assessing significant excursions (see Appendix A for details). There are five significant excursions, and the years of the most extreme part of each excursion are indicated on plot close to the corresponding value on the scatterplot.

in the scatterplot will rotate away from the 45° line in toward either the horizontal or vertical axes. There are three events (1812, 1815 and 1818) that fall close to the 45° line, all of which are associated with the Tambora event. Two other events are also noted at 1822 and 1886, both close to the vertical axis through the origin. The first of these is evidently part of the Tambora event that was still prominent in M20, but less so in MA20. The event at 1886 is due primarily to a large peak in M20, which is visible in the upper right-hand plot of Figure 4 (there is a vertical dotted line marking 1886). Below this plot is the one for MA20, which does have a peak around 1886 also, but displaced toward the date of the Krakatoa event (1883). Thus there is evidence of a significant local correlation between the M20 and MA20 around the time of the Krakatoa event if we ignore concerns about the dating of the two cores.

[31] **Acknowledgments.** We thank R. Mulvaney for assistance and thorough discussions on earlier versions of the manuscript and M. Kaczmarska (NPI) for sample preparation. We benefited from fruitful discussions with J.-O. Hagen (UIO), E. Isaksson (NPI), J. Kohler (NPI), J-G. Winther (NPI) and R. Hall (NPI). This work is a contribution to the 'European Project for Ice Coring in Antarctica' (EPICA), a joint ESF (European Science Foundation)/EC (European Commission) scientific program, funded by the EC and by national contributions from Belgium, Denmark, France, Germany, Italy, the Netherlands, Norway, Sweden, Switzerland, and the United Kingdom. This is EPICA Publication 161. This work was funded by the Research Council of Norway, the Norwegian Polar Institute and NSF Grant DMS-0222115.

References

Alley, R. B., et al. (1993), Abrupt increase in Greenland snow accumulation at the end of the Younger Dryas event, *Nature*, *362*, 527–529.

EPICA Community Members (2004), Eight glacial cycles from an Antarctic ice core, *Nature*, *429*, 623–628.

Fisher, D. A., N. Reeh, and H. B. Clausen (1985), Stratigraphic noise in time series derived from ice cores, *Ann. Glaciol.*, *7*, 76–83.

Hofstede, C. M., et al. (2004), Firn accumulation records for the past 1000 years on the basis of dielectric profiling of six cores from Dronning Maud Land, Antarctica, *J. Glaciol.*, *50*, 279–291.

Johnsen, S. J., H. B. Clausen, K. M. Cuffey, G. Hoffman, J. Schwander, and T. Creyts (2000), Diffusion of stable isotopes in polar firn and ice: the isotope effect in firn diffusion, in *Physics of Ice Core Records*, edited by T. Hondoh, pp. 121–140, Hokkaido Univ. Press, Sapporo, Japan.

Karlöf, L. (2004), Temporal and spatial variability of snow accumulation and redistribution, and its impact on the interpretation of ice cores, Ph.D. thesis, Univ. of Oslo, Oslo, Norway.

Karlöf, L., et al. (2000), A 1500-year record of accumulation at Amundsenisen western Dronning Maud Land, Antarctica, derived from electrical and radioactive measurements on a 120-m ice core, *J. Geophys. Res.*, *105*, 12,471–12,483.

Karlöf, L., et al. (2005), Accumulation variability over a small area in eastern Dronning Maud Land, Antarctica, as determined from shallow firn cores and snow pits: Some implications for ice core records, *J. Glaciol.*, *51*, 343–352.

Kay, S. M. (1981), Efficient generation of colored noise, *Proc. IEEE*, *69*, 480–481.

Kumar, P., and E. Foufoula-Georgiou (1997), Wavelet analysis for geophysical applications, *Rev. Geophys.*, *35*, 385–412.

Legrand, M., and P. A. Mayewski (1997), Glaciochemistry of polar ice cores: A review, *Rev. Geophys.*, *35*, 219–243.

Mayewski, P. A. (2003), Antarctic oversnow traverse-based Southern Hemisphere climate reconstruction, *Eos Trans. AGU*, *84*(22), 205, 210.

Mayewski, P. A., et al. (1994), Changes in atmospheric circulation and ocean ice cover over the North Atlantic during the last 41,000 years, *Science*, *263*, 1747–1751.

Moore, J. C., E. W. Wolff, H. B. Clausen, and C. U. Hammer (1992), The chemical basis for the electrical stratigraphy of ice, *J. Geophys. Res.*, *97*, 1887–1896.

Percival, D. B., and H. O. Mofjeld (1997), Analysis of subtidal coastal sea level fluctuations using wavelets, *J. Am. Stat. Assoc.*, *92*, 868–880.

Percival, D. B., and A. T. Walden (1993), *Spectral Analysis for Physical Applications: Multitaper and Conventional Univariate Techniques*, Cambridge Univ. Press, New York.

Percival, D. B., and A. T. Walden (2000), *Wavelet Methods for Time Series Analysis*, Cambridge Univ. Press, New York.

Petit, J. R., et al. (1999), Climate and atmospheric history of the past 420,000 years from the Vostok ice core, Antarctica, *Nature*, *399*, 429–436.

Rempel, A. W., and J. S. Wettlaufer (2003), Isotopic diffusion in polycrystalline ice, *J. Glaciol.*, *49*, 397–406.

Rempel, A. W., E. D. Waddington, J. S. Wettlaufer, and M. G. Worster (2001), Possible displacement of the climate signal in ancient ice by premelting and anomalous diffusion, *Nature*, *411*, 568–571.

Taylor, K. C., G. W. Lamorey, G. A. Doyle, R. B. Alley, P. M. Grootes, P. A. Mayewski, J. W. C. White, and L. K. Barlow (1993), The 'flickering switch' of late Pleistocene climate change, *Nature*, *361*, 432–436.

Taylor, K. C., et al. (2004), Dating the Siple Dome, Antarctica ice core by manual and computer interpretation of annual layering, *J. Glaciol.*, *50*, 453–461.

Whitcher, B. J., P. Guttorp, and D. B. Percival (2000), Wavelet analysis of covariance with application to atmospheric time series, *J. Geophys. Res.*, *105*, 14,941–14,962.

Winebrenner, D. P., R. J. Arthern, and C. A. Shuman (2001), Mapping Greenland accumulation rates using observations of thermal emission at 4.5-cm wavelength, *J. Geophys. Res.*, *106*, 33,919–33,934.

Winther, J. G., et al. (2002), European Project for ice coring in Antarctica (EPICA)—Nordic traverse in 2000/01, in *Report of the Norwegian Antarctic Research Expedition 2000–2001*, edited by J.-G. Winther, pp. 18–29, Norw. Polar Inst., Tromsø, Norway.

Wolff, E. W., J. C. Moore, H. B. Clausen, C. U. Hammer, J. Kipfstuhl, and K. Furhrer (1995), Long-term changes in the acid and salt concentrations of the Greenland Ice Core Project ice core from electrical stratigraphy, *J. Geophys. Res.*, *100*, 16,249–16,263.

L. Karlöf, Research and Development, Swix Sport AS, NO-2626 Lillehammer, Norway. (karlof@swixsport.no)

D. B. Percival and D. P. Winebrenner, Applied Physics Laboratory, Box 355640, University of Washington, Seattle, WA 98195-5640, USA.